Modeling local structure using crystal field and spin Hamiltonian parameters: the tetragonal Fe_K^{3+}–O_I^{2-} defect center in $KTaO_3$ crystal

2009 J. Phys.: Condens. Matter 21 455402

(http://iopscience.iop.org/0953-8984/21/45/455402)

J. Phys.: Condens. Matter **21** (2009) 455402 (11pp) doi:10.1088/0953-8984/21/45/455402

Modeling local structure using crystal field and spin Hamiltonian parameters: the tetragonal Fe_K^{3+}–O_I^{2-} defect center in $KTaO_3$ crystal

P Gnutek[1], Z Y Yang[2] and C Rudowicz[1,3]

[1] Institute of Physics, West Pomeranian University of Technology, Aleja Piastów 17, 70-310 Szczecin, Poland
[2] Department of Physics, Baoji University of Arts and Science, Baoji 721007, People's Republic of China

E-mail: crudowicz@zut.edu.pl

Received 5 August 2009, in final form 3 October 2009
Published 23 October 2009
Online at stacks.iop.org/JPhysCM/21/455402

Abstract

The local structure and the spin Hamiltonian (SH) parameters, including the zero-field-splitting (ZFS) parameters D and $(a + 2F/3)$, and the Zeeman g factors $g_\parallel$ and $g_\perp$, are theoretically investigated for the Fe_K^{3+}–O_I^{2-} center in $KTaO_3$ crystal. The microscopic SH (MSH) parameters are modeled within the framework of the crystal field (CF) theory employing the CF analysis (CFA) package, which also incorporates the MSH modules. Our approach takes into account the spin–orbit interaction as well as the spin–spin and spin–other-orbit interactions omitted in previous studies. The superposition model (SPM) calculations are carried out to provide input CF parameters for the CFA/MSH package. The combined SPM-CFA/MSH approach is used to consider various structural models for the Fe_K^{3+}–O_I^{2-} defect center in $KTaO_3$. This modeling reveals that the off-center displacement of the Fe^{3+} ions, $\Delta_1(Fe^{3+})$, combined with an inward relaxation of the nearest oxygen ligands, $\Delta_2(O^{2-})$, and the existence of the interstitial oxygen O_I^{2-} give rise to a strong tetragonal crystal field. This finding may explain the large ZFS experimentally observed for the Fe_K^{3+}–O_I^{2-} center in $KTaO_3$. Matching the theoretical MSH predictions with the available structural data as well as electron magnetic resonance (EMR) and optical spectroscopy data enables predicting reasonable ranges of values of $\Delta_1(Fe^{3+})$ and $\Delta_2(O^{2-})$ as well as the possible location of O_I^{2-} ligands around Fe^{3+} ions in $KTaO_3$. The defect structure model obtained using the SPM-CFA/MSH approach reproduces very well the ranges of the experimental SH parameters D, $g_\parallel$ and $g_\perp$ and importantly yields not only the correct magnitude of D but also the sign, unlike previous studies. More reliable predictions may be achieved when experimental data on $(a + 2F/3)$ and/or crystal field energy levels become available. Comparison of our results with those arising from alternative models existing in the literature indicates considerable advantages of our method and presumably higher reliability of our predictions.

1. Introduction

The relaxational properties and defect structure of the pure and transition-metal-doped $KTaO_3$, which serves as a model quantum paraelectric, have been reviewed by Samara [1]. A perfect $KTaO_3$ crystal has cubic structure resulting in cubic site symmetry around the cations, namely the 6-fold cubic coordination for Ta^{5+} sites, whereas it has 12-fold cubic coordination for K^+ sites (see figure 1) [2, 3]. Trivalent Fe^{3+} ions doped in $KTaO_3$ crystal can substitute for both

[3] Author to whom any correspondence should be addressed.

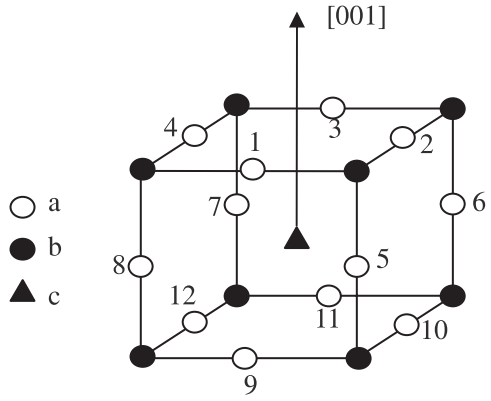

Figure 1. The local environment of the K^+ ion in the 12-fold cubic coordination in the host $KTaO_3$ crystal: (a) O^{2-} ions, (b) Ta^{2+} ions, (c) K^+ ions.

Ta^{5+} and K^+ ions [4–6]. However, in addition to the two cubic sites, two axial (tetragonal) defect sites have been observed in EMR spectra [4, 7]. These Fe^{3+} sites are characterized by surprisingly large values of the second-rank axial zero-field-splitting (ZFS) parameter D. The values $D = 4.30$ cm^{-1} [8], $D = 4.44 \pm 0.014$ cm^{-1} (and $g = 1.92 \pm 0.02$) [5] and $D = 4.46$ cm^{-1} (independently determined in [9] and [10]) were assigned to the Fe_K^{3+}–O_I^{2-} defect centers, where O_I^{2-} denotes an oxygen ion on the nearest interstitial site acting as a compensator for the Fe_K^{3+} center. The values $D = 1.33$ cm^{-1} at room temperature and 1.44 cm^{-1} at 77 K [9] were assigned to the Fe_{Ta}^{3+}–V_O defect center [5, 7, 9], where V_O denotes an oxygen vacancy acting as the nearest-neighbor compensator. Bykov *et al* [9] have determined that D does not depend on temperature for the former center, whereas it reduces linearly with temperature for the latter center. The site assignments were confirmed by the optically detected magnetic resonance and the magnetic circular dichroism [6, 11]. Structural models proposed by Laguta *et al* [7] for the two axial Fe^{3+} centers have been confirmed by the authors' ENDOR studies and additionally by the electric-field-induced orientation studies by Sochava *et al* [12] for the Fe_K^{3+}–O_I^{2-} center. Note that the $KTaO_3$ lattice allows six possible orientations for the Fe_K^{3+}–O_I^{2-} center [12]. A controversy exists in the literature concerning the sign of D for the Fe_K^{3+}–O_I^{2-} center. The sign of $D = 4.46$ cm^{-1} has unequivocally been determined experimentally as positive [9, 10], and thus represented as such by other authors, see, e.g., [4, 6, 7, 13–15]. However, in a recent paper Zheng *et al* [16] have claimed that Bykov *et al* [9] did not determine the sign of D. The authors [16] have compared their negative theoretical values of D with the alleged experimental value $D_{expt} = -4.46$ cm^{-1}, just disregarding the bulk of experimental evidence [4, 6, 7, 9, 10, 13–15].

In order to interpret the EMR results within the framework of crystal field (CF) theory [17–21] and microscopic spin Hamiltonian (SH) theory [22–26], the values of the physical parameters need to be determined. For Fe^{3+} ions in $KTaO_3$ the cubic CF at the K^+ site ($Dq = 1230$ cm^{-1}, so for the 6-fold cubic coordination—see later) [27] appears to be much weaker than that at the Ta^{5+} site ($Dq = 1600$ cm^{-1}) [28]. Hence, for Fe^{3+} ions at the K^+ sites, i.e. the Fe_K^{3+} centers, one would expect a value of the ZFS parameter D smaller than that for Fe^{3+} ions at the Ta^{5+} sites, i.e. the Fe_{Ta}^{3+} centers. However, the experiments [5, 8–10] show that the D values for the Fe_K^{3+} center are remarkably larger in magnitude than those for the Fe_{Ta}^{3+} center. The ionic radius of Fe^{3+} ($R_{Fe} = 0.064$ nm) is approximately half that of K^+ ($R_K = 0.133$ nm) [29] and the K^+ ion is replaced by an impurity Fe^{3+} ion having different charge. The force acting on the impurity Fe^{3+} should differ from that acting on the host ion. Hence, Laguta *et al* [13] suggested that Fe^{3+} ions may move along the c axis in $KTaO_3$ and the resultant interstice may be occupied by an additional O^{2-} (hereafter denoted O_I^{2-}), thus providing the required charge compensation. To calculate theoretically the large value of D for Fe^{3+} ions at the K^+ sites, Zhou [30] employed the spin–orbit interaction [31–33] and the superposition model [21, 34–36]. The contribution from O_I^{2-} to the ZFS parameter D was found [30] to decrease rather than increase the total D. Hence, according to Zhou [30] although the presence of O_I^{2-} in the vicinity of Fe^{3+} seems to account reasonably for the charge compensation, this model [30] fails to explain the observed D values. Alternatively, Zhou [30] proposed assuming an off-center displacement of the Fe^{3+} ion $\Delta_1(Fe^{3+})$ combined with a considerable inward relaxation of the oxygen ligands $\Delta_2(O^{2-})$ of about 0.03 nm. The model [30] seems capable of explaining the value $D_{expt} = 4.46$ cm^{-1} for the Fe_K^{3+} centers without invoking the presence of the interstitial O_I^{2-}. Zhou's paper [30] was critically commented on by Donnerberg *et al* [37] and Zheng [38]. Zheng [38] asserts that if equations (2), (3) or (4) of [30] are used, the displacement $\Delta_2(O^{2-}) = 0.03$ nm is not sufficient to explain the large value of D and hence the presence of O_I^{2-} cannot be excluded. The above controversies as well as our recent Science Citation Index search indicate that no satisfactory theoretical explanation of the existing experimental EMR findings for the Fe_K^{3+}–O_I^{2-} center in $KTaO_3$ is available yet.

This paper is aimed at solving the D sign controversy and providing a better understanding of the relationships between the local structure and the SH parameters for the Fe_K^{3+}–O_I^{2-} defect center in $KTaO_3$ crystal. To this end we utilize the superposition model of CF parameters [17–21, 34–36] and the microscopic SH theory [22–26]. Since experimental work [6, 13, 39] favors the idea that the interstitial defect oxygen is responsible for the strong axial character of this center, we attempt to corroborate this model. Note that EMR and dielectric measurements on samples with different Fe^{3+} concentrations have confirmed the decisive role of the complex Fe_K^{3+}–O_I^{2-} [40, 41]. The origin of dielectric losses in Fe:$KTaO_3$ at $T \cong 185$ K has been ascribed [41] to the reorientational motion of the dipole complex Fe_K^{3+}–O_I^{2-}. Subsequently, we consider the following three mechanisms contributing to the tetragonal (C_{4v}) crystal field acting on the Fe^{3+} ions forming the Fe_K^{3+}–O_I^{2-} centers in $KTaO_3$ (see figure 2): (a) the nearest-neighbor interstitial oxygen O_I^{2-} arising from the charge compensation along the C_4 axis; (b) the electrostatic attraction Fe^{3+}–O^{2-}, i.e. between the Fe^{3+} ion and the nearest eight

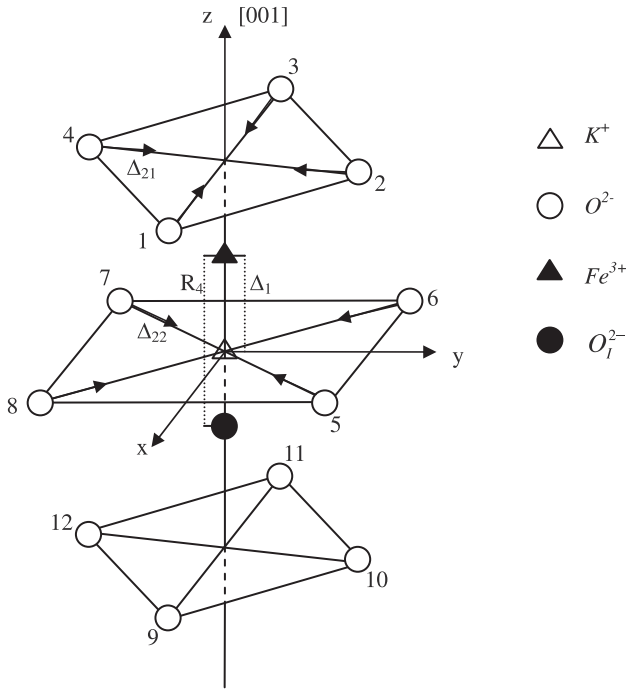

Figure 2. The local structure of an off-center Fe^{3+} ion at the K^+ site in $KTaO_3$; one of the possible six orientations of the Fe–O complex in the unit cell is shown.

O^{2-} ligands, which is much stronger than the attraction K^+–O^{2-} due to the larger charge on Fe^{3+} and thus could cause an off-center displacement of the Fe^{3+} ion and (c) the inward relaxation of the nearest-neighbor oxygens (O_1–O_{12}) arising from the differences in the mass and radius between the Fe^{3+} and K^+ ions. The model of the local structure of an off-center Fe^{3+} ion at the K^+ site in $KTaO_3$ defined by the three mechanisms (a)–(c) is depicted in figure 2.

Our theoretical approach employs the superposition model (SPM) [21, 34–36] to calculate the CF parameters, whereas the complete diagonalization method, which underlies the extended CF analysis (CFA) package incorporating also the microscopic SH (MSH) modules [42–44], is used to model the optical energy levels and/or the SH parameters. Based on the structural model outlined above, the combined SPM-CFA/MSH approach enables us to establish the relationships between the defect structure parameters for the Fe_K^{3+}–O_I^{2-} center in $KTaO_3$ on the one hand and the SH parameters D, $(a + 2F/3)$, $g_\parallel$ and $g_\perp$ on the other hand. The variations of the SH parameters with the structural model parameters have been investigated taking into account the effect of the inward relaxation of the nearest-neighbor oxygen ligands, the oxygen interstitials O_I^{2-} themselves and the off-center displacement of the Fe^{3+} ion. The available experimental [8–10] data on D, $g_\parallel$ and $g_\perp$ may not be accurate enough to serve as an acid test of our theoretical predictions. Nevertheless, the SPM-CFA/MSH approach to defect structure modeling proves capable of matching well the experimental SH parameters with the theoretical predictions. More precise results may be obtained if more accurate experimental data, including EMR data on the fourth-rank ZFS parameters and/or crystal field energy levels not yet determined, become available.

2. Basic crystal field and spin Hamiltonian theory

The crystal field analysis (CFA) and microscopic spin Hamiltonian (MSH) package CFA/MSH developed by us was previously employed for the $3d^2$ ($3d^8$) [42, 43, 45, 46] and $3d^3$ ($3d^8$) [47] ions at trigonal symmetry sites [47]. In the present work we utilize the package CFA/MSH based on the complete diagonalization method (CDM) and apply it for the $3d^5$ ions at tetragonal symmetry CF. The total Hamiltonian is given by

$$H = H_{ee}(B, C) + H_{\mathrm{CF}}(B_{kq}) + H_{\mathrm{m}}(\xi_d, M_0, M_2), \quad (1)$$

where the respective terms represent the Coulomb interactions, CF, and magnetic interactions [45] that include, apart from the spin–orbit (SO) interaction, also the spin–other-orbit (SOO) and spin–spin (SS) interactions [48, 49]:

$$H_{\mathrm{m}} = H_{\mathrm{so}}(\xi_d) + H_{\mathrm{soo}}(M_0, M_2) + H_{\mathrm{ss}}(M_0, M_2). \quad (2)$$

Explicit forms of the terms in equation (2) have been given in equations (2)–(4) in [45].

The CFA/MSH package constructs the complete 252×252 energy matrix for the $3d^5$ ions at tetragonal symmetry sites and, *for the first time*, incorporates the SS and SOO interactions omitted in the previous studies [50–53]. The complete energy matrix can be partitioned into four smaller matrices, i.e. $E'\alpha'(62 \times 62)$, $E'\beta'(62 \times 62)$, $E''\alpha''(64 \times 64)$ and $E''\beta''(64 \times 64)$. Details concerning the choice of the basis of states and calculations of the pertinent matrix elements have been published previously [45, 54, 55]. The Hamiltonian matrices obtained in this way are the functions of the Racah parameters B and C, the CF parameters B_{kq} (in the Wybourne notation [17]), the SO constant ξ_d, and the SS and SOO parameters M_0, M_2. Provided the values of these microscopic parameters are available, diagonalization of the full Hamiltonian matrices yields the energy levels and eigenvectors. The ground state $3d^5(^6S)$ eigenvectors obtained using the CDM include admixtures of the excited states arising from various ^{2S+1}L multiplets [45, 54]. These eigenvectors are used in the calculations of the MSH parameters based on the procedure outlined in [42].

In general, the *effective* SH [25, 26], including the Zeeman term and the ZFS term, may be expressed either in the conventional notation or in one of the two types of tensor operator notations [25, 26, 56]. For $3d^5$ ions at tetragonal symmetry sites, the explicit form of SH with the ZFS terms expressed in the extended Stevens operator (ESO) notation [57] is

$$H_S = \mu_{\mathrm{B}} g_\parallel B_z S_z + \mu_{\mathrm{B}} g_\perp (B_x S_x + B_y S_y) + B_2^0 O_2^0 + B_4^0 O_4^0 + B_4^4 O_4^4 \quad (3)$$

with the ES operators $O_k^q(S_x, S_y, S_z)$ expressed in the axis system with the tetragonal z axis and the x and y axes along two perpendicular twofold axes (or the two symmetry plane traces). The choice of C_2 or C_2' axes as the x and y axes remains arbitrary. Since a rotation 45° about the z axis leaves

the form of (3) unchanged but induces a sign change of B_4^4, an ambiguity arises in the experimentally determined signs of B_4^4 unless the axis system used is clearly specified with respect to the crystallographic axes. Since the conventional ZFS parameters [22, 25, 26, 56] (D, a and F) are predominantly employed in EMR studies of transition ions in $KTaO_3$, we provide the conversion relations:

$$B_2^0 = \frac{1}{3}D, \qquad B_4^0 = \frac{a}{120} + \frac{F}{180},$$
$$B_4^4 = \frac{a}{24} \qquad \text{or} \qquad b_2^0 = D, \tag{4}$$
$$b_4^0 = \frac{a}{2} + \frac{F}{3}, \qquad b_4^4 = \frac{5}{2}a.$$

The microscopic spin Hamiltonian theory [22, 25, 26] enables us to derive explicit expressions for the *effective* SH parameters in equation (3) in terms of the energy separations obtained by the diagonalization of the *physical* Hamiltonian in equations (1) and (2). The equivalence of the energy levels of the *physical* Hamiltonian and those of the *effective* one is used to derive the expressions for the ZFS parameters [22, 25, 26]. However, for $3d^5$ ions in tetragonal CF, the number of available ZFS transitions within the ground spin $S = 5/2$ state obtained from the CDM is only two, whereas that of the non-zero ZFS parameters is three. Hence, it is not feasible to determine analytically all non-zero ZFS parameters and some approximations must be made. If the mixing coefficient [56] between the *effective* spin states [25, 26] $\Psi_{\tilde{M}_S} = |\tilde{M}_S\rangle$ of H_S in equation (3) in the absence of external magnetic field, $\tan 2\gamma = (\sqrt{5}a)/[(a + 2F/3) + 4D]$, is very small, we obtain approximate expressions for the ZFS parameters D and $(a + 2F/3)$ in the form

$$D \approx \tfrac{1}{28}(4\delta_1 + 5\delta_2) \tag{5a}$$

$$a + 2F/3 \approx \tfrac{1}{7}(\delta_2 - 2\delta_1) \tag{5b}$$

where δ_1 and δ_2 are the energy separations between the *effective* spin states defined as

$$\delta_1 = E(|\tilde{M}_S = \pm 3/2\rangle) - E(|\tilde{M}_S = \pm 1/2\rangle);$$
$$\delta_2 = E(|\tilde{M}_S = \pm 5/2\rangle) - E(|\tilde{M}_S = \pm 3/2\rangle). \tag{5c}$$

The parametric relations for δ_1 and δ_2 are obtained by the diagonalization of the energy matrices within the full $3d^5$ configuration. Comparing the experimental [4, 6, 7, 9, 13–15] values $D = 4.46\ \text{cm}^{-1}$ for Fe_K^{3+}–O_I^{2-} and the only available value $a = 0.0030\ \text{cm}^{-1}$ [58] for Fe_K^{3+} at the cubic site in $KTaO_3$ or $a \cong 0.0090\ \text{cm}^{-1}$ (see table I in [59]) for Fe^{3+} at the cubic and tetragonal sites in $BaTiO_3$ it may be safely assumed that the relation: $4D \gg a$ would be well obeyed in the present case. Hence, $\tan 2\gamma$ is indeed very small and the expressions in equations (5) constitute a satisfactory approximation.

The microscopic expressions for the g factors are obtained by means of the matrix element equivalence [23, 25, 26] between the *effective* Zeeman term in equation (3) and the *physical* one as follows:

- for the $|\tilde{M}_S = \pm 1/2\rangle$ ground state:

$$g_\parallel = 2\{k\langle\Psi_{+1/2}|L_0^{(1)}|\Psi_{+1/2}\rangle + g_e\langle\Psi_{+1/2}|S_0^{(1)}|\Psi_{+1/2}\rangle\} \tag{6a}$$

$$g_\perp = \frac{\sqrt{2}}{3}\{k(\langle\Psi_{+1/2}|L_{-1}^{(1)}|\Psi_{-1/2}\rangle - \langle\Psi_{+1/2}|L_{+1}^{(1)}|\Psi_{-1/2}\rangle) + g_e(\langle\Psi_{+1/2}|S_{-1}^{(1)}|\Psi_{-1/2}\rangle - \langle\Psi_{+1/2}|S_{+1}^{(1)}|\Psi_{-1/2}\rangle)\} \tag{6b}$$

- for the $|\tilde{M}_S = \pm 5/2\rangle$ ground state:

$$g_\parallel = \tfrac{2}{5}\{k\langle\Psi_{+5/2}|L_0^{(1)}|\Psi_{+5/2}\rangle + g_e\langle\Psi_{+5/2}|S_0^{(1)}|\Psi_{+5/2}\rangle\} \tag{6c}$$

$$g_\perp = \frac{\sqrt{2}}{\sqrt{5}}\{k(\langle\Psi_{+5/2}|L_{-1}^{(1)}|\Psi_{+3/2}\rangle - \langle\Psi_{+5/2}|L_{+1}^{(1)}|\Psi_{+3/2}\rangle) + g_e(\langle\Psi_{+5/2}|S_{-1}^{(1)}|\Psi_{+3/2}\rangle - \langle\Psi_{+5/2}|S_{+1}^{(1)}|\Psi_{+3/2}\rangle)\}. \tag{6d}$$

In equations (6) k is the orbital reduction factor for the orbital angular momentum $\boldsymbol{L}$, whereas the *physical* eigenfunctions $\Psi_{\pm M_S}$ are denoted by the dominant component $|\pm M_S\rangle$ of the ^6S ground multiplet and are distinct from the *effective* [25, 56] spin states $\Psi_{\tilde{M}_S}$. The functions $\Psi_{\pm M_S}$ are, in fact, appropriate linear combinations of the *physical* eigenfunctions within the whole $3d^5$ configuration. The explicit forms of $\Psi_{\pm M_S}$ are obtained by the CDM and are subsequently used within the MSH module of the CFA/MSH package. The matrix elements of the irreducible tensor operators in equations (6) are computed using the Wigner–Eckart theorem [42, 60].

A crucial point concerns the sign of D for the spin $S = 5/2$ systems. It is well established that the ground state $|\tilde{M}_S = \pm 1/2\rangle$ of H_S in (3) in zero magnetic field corresponds to $D > 0$, whereas $|\tilde{M}_S = \pm 5/2\rangle$ corresponds to $D < 0$ (see, e.g., [56, 22, 23]). Correspondingly, equation (2) yields positive and negative D for the ground state $|\tilde{M}_S = \pm 1/2\rangle$ and $|\tilde{M}_S = \pm 5/2\rangle$, respectively. In general, the sign of D may be experimentally determined from the variation of the intensity of the resonance lines at low temperature (see, e.g., [56, 22, 23]). The observed EMR transitions in the range $g\mu_B B \ll D$ for the two axial Fe^{3+} centers [9, 14, 15] Fe_{Ta}^{3+}–V_O and Fe_K^{3+}–O_I^{2-} as well as for the rhombic [15, 61, 62] Fe_{Ta}^{3+} center (with $D = 0.44\ \text{cm}^{-1}$ [15]) in $KTaO_3$ have been identified as due to the transitions between the states of the *lowest* Kramers doublet $|\tilde{M}_S = \pm 1/2\rangle$. Hence, in view of the ample experimental EMR data [4, 6, 7, 13–15], the sign of the experimental value D for the center Fe_K^{3+}–O_I^{2-}, e.g. cited by Zheng *et al* [16] as $D = |4.46|\ \text{cm}^{-1}$, may be considered as unequivocally determined to be positive. Note that the ZFS parameters D and E (b_2^0 and b_2^2) were named inappropriately as *'crystal field'* parameters in some $KTaO_3$-related papers [9, 15, 61, 62]. As argued in the reviews [25, 26, 63] such terminology confuses two distinct physical quantities: (i) the *actual* CF Hamiltonian and (ii) the *effective* ZFS (or fine structure) Hamiltonian as well as the respective CF and ZFS parameters. Unfortunately, this confusion is widely spread in EMR [25, 26, 59, 63] and magnetism [64, 65] literature.

3. Structural defect model and CF parameters

For Fe_K^{3+} in $KTaO_3$ crystal the following values of the *physical* parameters have been obtained [27] from optical spectra: $B = 690$, $C = 3452$ and the cubic CF parameter for the 6-fold cubic coordination $Dq = 1230$ (in cm^{-1}). To evaluate the orbital reduction factor k and the spin–orbit coupling constant ξ_d, we use the relation [66, 67] $N^2 \approx (\sqrt{B/B_0} + \sqrt{C/C_0})/2$, where $B_0 = 1015\ cm^{-1}$, $C_0 = 4800\ cm^{-1}$ are the Racah parameters of a free Fe^{3+} ion [18]. Thus, we obtain $k \approx N^2 \approx 0.84$ and, using the free Fe^{3+} ion value [19] $\xi_0 = 499.5\ cm^{-1}$, $\xi_d \approx N^2\xi_0 = 420\ cm^{-1}$. The SS or SOO parameters $M_0 = 0.2917\ cm^{-1}$ and $M_2 = 0.0229\ cm^{-1}$ for $Fe^{3+}(3d^5)$ ions are adopted in our calculations [68]. Having fixed the values of the microscopic parameters B, C, ξ_d, M_0, M_2 and k, the theoretically predicted SH parameters, i.e. D, a, F, $g_\parallel$ and $g_\perp$, become functions of only the CF parameters B_{20}, B_{40} and B_{44}, which in turn may be directly related to the structure of the Fe_K^{3+}–O_I^{2-} complex. Hence, the theoretical SH and structural parameters can be modeled via the SPM/CF parameters and then compared with the experimentally measured SH ones. This enables verification of the theoretical predictions and selection of the structural model describing best the given paramagnetic center.

Our model of the Fe_K^{3+}–O_I^{2-} defect center, outlined in section 1, is characterized by the following quantities shown in figure 2: the distance R_4 of the interstitial oxygen O_I^{2-} from the Fe^{3+} ion, the deviation $\Delta_1(Fe^{3+})$ from the ideal K^+ site, the inward relaxation of the nearest-neighbor (O_1–O_{12}) oxygen ligands, i.e. the deviation $\Delta_2(O^{2-})$, the inward relaxation of the nearest-neighbor oxygens in a given plane: (1) the upper oxygen (O_1–O_4) plane: the deviation $\Delta_{21}(O^{2-})$, (2) the middle (O_5–O_8) plane: $\Delta_{22}(O^{2-})$, and (3) the lower (O_9–O_{12}) plane: $\Delta_{23}(O^{2-})$. The values of all deviations considered in our calculations are measured in units of $a/2$, where the lattice constant $a = 0.398\,85$ nm. Using the local structure of an off-center Fe^{3+} ion at the K^+ site in $KTaO_3$ (figure 2) and the expressions for the coordination factors [69] within the SPM framework [21, 34–36] we derive the following geometrical relationship for the non-zero CF parameters B_{kq} appropriate for C_{4v} site symmetry:

$$B_{20} = 4\bar{A}_2 \sum_{i=1}^{3}\left(\frac{R_0}{R_i}\right)^{t_2}[3\cos^2\theta_i - 1] + 2\bar{A}_2\left(\frac{R_0}{R_4}\right)^{t_2} \tag{7a}$$

$$B_{40} = 4\bar{A}_4 \sum_{i=1}^{3}\left(\frac{R_0}{R_i}\right)^{t_4}[35\cos^4\theta_i - 30\cos^2\theta_i + 3] + 8\bar{A}_4\left(\frac{R_0}{R_4}\right)^{t_4} \tag{7b}$$

$$B_{44} = 32\sqrt{\frac{35}{128}}\bar{A}_4 \sum_{i=1}^{3}\left(\frac{R_0}{R_i}\right)^{t_4}\sin^4\theta_i \exp(-\mathrm{i}4\varphi_i) \tag{7c}$$

where R_0 is the reference distance [34–36]. In equations (7) the summation is over the upper (1), middle (2) and lower (3) oxygen planes (see figure 2), whereas the interstitial oxygens O_I^{2-} at the distance R_4 from Fe^{3+} yield contributions only to the axial CF parameters, while the azimuthal angles φ_i involved in equation (7*c*) can be read out from figure 2 (see later). Referring to the local structure in figure 2, we define the structural parameters as follows:

$$R_1 = \frac{a}{2}\sqrt{(1-\Delta_1)^2 + (1-\Delta_{21})^2},$$
$$R_2 = \frac{a}{2}\sqrt{\Delta_1^2 + (\sqrt{2}-\Delta_{22})^2}, \tag{8a}$$
$$R_3 = \frac{a}{2}\sqrt{(1+\Delta_1)^2 + 1}$$

$$\cos\theta_1 = \frac{a}{2}\frac{(1-\Delta_1)}{R_1}, \qquad \cos\theta_2 = \frac{a}{2}\frac{\Delta_1}{R_2}, \qquad \cos\theta_3 = \frac{a}{2}\frac{(1+\Delta_1)}{R_3}. \tag{8b}$$

In the case of another $3d^5$ ion center, i.e. Mn_K^{2+} in $KTaO_3$, it was found [2] that the next-nearest-neighbor oxygens (O_9–O_{12}) provide only a small contribution to the MSH parameter D for the off-center displacement of the Mn^{2+} ion from the ideal K^+ site $\Delta_{Mn} > 0.4$. For this center the deviation Δ_{Mn} was estimated [2] as 0.50–0.64, indicating that the Mn^{2+} ions were located in between the upper and middle oxygen planes. Thus, the inward relaxation of the (O_9–O_{12}) oxygens is not considered in our structural model. The quantities $\bar{A}_2(R_0)$ and $\bar{A}_4(R_0)$ in equations (7) are the intrinsic SPM parameters [21, 34–36]. The ratio $\bar{A}_2(R_0)/\bar{A}_4(R_0)$ tends to be a constant of about 11 for $3d^N$ ions [70–72]. It is taken as 10.8 in our calculations.

We note that the parameter $\bar{A}_4(R_0)$ is independent of the coordination: however, calculations must be carried out using data consistently for a given coordination. Since the value of the cubic CF parameter Dq reported by Bryknar's *et al* [27] was obtained using the Tanabe–Sugano diagram assuming 6-fold cubic coordination, the considerations below must be carried out for the 6-fold cubic coordination instead of the 12-fold one. For $3d^N$ ions in the 6-fold cubic coordination, $\bar{A}_4(R_0)$ can be found from the relation [36]: $\bar{A}_4 = 3Dq/4$. Using $Dq(R_0) = 1230\ cm^{-1}$ for Fe^{3+} ions at the K^+ sites in the $KTaO_3$ crystal [27] yields $\bar{A}_4(R_0) = 922.5\ cm^{-1}$. Using the relation [73]: $Dq(R_0)R_0^5 = Dq(R)R^5$, with $R = a/2 = 0.1994$ nm taken [37] as the Fe^{3+}–O^{2-} distance in the perfect cubic 6-fold Ta^{5+} site in $KTaO_3$ and $Dq(R) = 1600\ cm^{-1}$ for Fe^{3+} at this site [28], we obtain $R_0 \approx 1.054a/2 = 0.2102$ nm. The SPM power-law exponents $t_2 = 3$ and $t_4 = 5$ are adopted in our calculations as the values suitable for ionic bonds [21, 34–36].

For the Fe_K^{3+}–O_I^{2-} defect center, the interstitial oxygen O_I^{2-} and the off-center impurity Fe^{3+} may move closer to each other along the C_4 axis due to the electrostatic attraction. This would result in formation of a considerable covalent bonding between Fe^{3+} and O_I^{2-}, and thus the bond length R_4 could be smaller than the sum of the ionic radii $r_{O^{2-}}$ (=0.132 nm) and $r_{Fe^{3+}}$ (=0.064 nm). This point is partially supported by the data [74] on another trivalent ion Ni^{3+} substituting for K^+ in $KTaO_3$ (studied recently by EMR [75]) where the covalent bond length $R(Ni_K^{3+}$–$O_I^{2-})$ is found to be about 0.176(8) nm. This means that the bond length for Ni_K^{3+}–O_I^{2-} is smaller by about 0.019 nm than the sum of radii $r_{O^{2-}}$ (=0.132 nm) and $r_{Ni^{3+}}$ (=0.063 nm). Hence, in view of the above values of

$r_{Fe^{3+}}$ and $r_{O^{2-}}$, the bond length R_4 between Fe^{3+} and O_I^{2-} is taken approximately in our calculations as 0.181 nm, which is comparable to 0.183 nm used by Donnerberg [37] for the Fe_K^{3+}–O_I^{2-} defect center in $KTaO_3$.

4. Results and discussion

The modeling procedure developed in section 3 enables us to obtain insight into the variation of the SH parameters with the structural model parameters: $\Delta_1(Fe^{3+})$—the off-center displacement of the Fe^{3+} ions, and $\Delta_2(O^{2-})$—the inward relaxation of the nearest oxygen ligands, e.g. $\Delta_{21}(O^{2-})$ for the upper (1) oxygen plane and $\Delta_{22}(O^{2-})$ for the middle (2) oxygen plane. The ZFS parameter D was calculated in this way as a function of the structural model parameters and compared with the experimental [9, 10] value $D(Fe_K^{3+}–O_I^{2-}) = 4.46\ cm^{-1}$. This procedure enables us to optimize the geometry by matching the experimental value of D with that calculated theoretically by varying the structural parameters, which in turn affect the CF parameters, while adopting reasonable values of the free-ion parameters and the superposition model ones as discussed in section 3. It turns out that D is very sensitive to the changes in $\Delta_1(Fe^{3+})$ for Δ_1 above 0.6, whereas it is insensitive below. The theoretical values of the SH parameters D, $g_\parallel$ and $g_\perp$ fall very well within the error limits of the values determined experimentally. Comparison of the predicted values of $(a + 2F/3)$, for which no experimental data for the Fe_K^{3+}–O_I^{2-} center in $KTaO_3$ is available, with those determined for Fe^{3+} ions in similar compounds, e.g. for Fe^{3+} at the tetragonal sites [59] in $BaTiO_3$, indicates that these values also fall into a reasonable range.

SPM calculations were carried out in the range 0–0.9 for $\Delta_1(Fe^{3+})$, whereas 0–0.20 for $\Delta_{21}(O^{2-})$ and $\Delta_{22}(O^{2-})$. These ranges arise from the physical feasibility of the distortions in question. Note that the zero values correspond to a cubic symmetry case, whereas further increase of Δ_{21} and Δ_{22} above the adopted limits would result in overlapping of ligands. The results reveal that best agreement for the ZFS parameter D can be achieved for $\Delta_1(Fe^{3+}) = 0.73$ and $\Delta_{21}(O^{2-}) = 0.15$. SPM calculations show also that the displacement of oxygens towards the center of the middle plane yields a reduction of the D value, hence we adopt $\Delta_{22}(O^{2-}) = 0$ and below we use $\Delta_2(O^{2-})$ instead of $\Delta_{21}(O^{2-})$. It is worth pointing out that the large off-center displacement Δ_1 has also been obtained using the SPM applied for the SH parameters [2, 34–36] and the generalized gradient approximation (GGA) [76] for other transition ion centers in $KTaO_3$:$\Delta_1(Mn_K^{2+}) = 0.50$–$0.64$ [2], 0.45 [40, 41], $\Delta_1(Cu_K^{2+}) = 0.70$ [76] and $\Delta_1(Co_K^{2+}) = 0.59$ [76]. In view of these results, the large off-center displacement determined by us: $\Delta_1(Fe^{3+}) = 0.73$ for Fe_K^{3+} ions in $KTaO_3$ crystal, seems fully acceptable. The substantial inward relaxation for the nearest oxygens determined by us is also reasonable, keeping in mind the large difference of the ionic radius of Fe^{3+} (0.064 nm) and K^+ (0.133 nm). This outcome is also supported by the calculations based on the GGA method [76] and the superposition model [30].

Additionally, our model CFA/MSH calculations indicate that, if the interstitial oxygen O_I^{2-} is excluded from calculations, then the ground state of the Fe_K^{3+} ion in $KTaO_3$ would be the spin-quadruplet with $S = 3/2$ rather than the experimentally observed spin-sixtet with $S = 5/2$. Such an $S = 3/2$ ground state may originate from the higher lying multiplet $^4G(^4T_{1g})$ lowering in energy in strong tetragonal CF. This result implies that the contribution to the ZFS parameter D from the interstitial oxygen O_I^{2-} located nearby the Fe_K^{3+} center in $KTaO_3$ is significant and shall be taken into account. Recently Baranov *et al* [77] studied by X-band EMR the hyperfine and superhyperfine interactions for the three iron-related centers in ^{57}Fe-doped $KTaO_3$, namely (i) rhombic ($S = 5/2$), (ii) Fe_K^{3+}–O_I^{2-}, labeled also $Fe\frac{6}{2}$, and (iii) $Fe\frac{4}{2}$. The center (ii) was described [77] as 'axial center Fe_K^{3+}–O_I^{2-} at the K site with two adjoining O vacancies', which exhibits a strong axial crystal field on the Fe_K^{3+} ($S = 5/2$) ion, resulting in an effective spin $S_{eff} = 1/2$. Such a description contradicts the generally accepted [4, 6, 7, 13–15] nature of the Fe_K^{3+}–O_I^{2-} center as associated with the interstitial oxygen O_I^{2-}. Concerning the center a few points may be mentioned. This center originates [77] from an $S = 3/2$ system experiencing a strong axial crystal field resulting in a Kramers $S_{eff} = 1/2$ ground state. However, the $Fe\frac{4}{2}$ center has not been assigned in [77] to a specific ion and specific charge state. Hence, it is feasible that, from several options considered in [77], our model CFA/MSH calculations indicating the possibility of the Fe_K^{3+} ($S = 3/2$) centers for specific values of the microscopic model parameters may be a viable option.

In table 1 we list the SH parameters calculated for the five model cases considered. These results indicate that relaxation of the oxygen ions in the vicinity of Fe_K^{3+} is most likely to occur and plays a significant role in contributing to the ZFS parameter D. In fact, the zero value of D is obtained for case (A) in table 1 with $\Delta_1(Fe^{3+}) = \Delta_2(O^{2-}) = 0$ and the interstitial oxygen O_I^{2-} excluded from calculations. Cases (B) and (C) in table 1 include the displacement of the Fe^{3+} ion $\Delta_1(Fe^{3+}) = 0.73$, the inward relaxation of the nearest oxygen $\Delta_2(O^{2-}) = 0.15$ and assume the existence of an interstitial oxygen O_I^{2-} in the vicinity of the Fe^{3+} ion. The combined theoretical contributions to the SH parameters (table 1 cases (B) and (C)) due to these three mechanisms yield the correct sign of D and cover very well the range of experimental values of D, $g_\parallel$ and $g_\perp$. This finding corroborates the model of the Fe_K^{3+}–O_I^{2-} defect center in $KTaO_3$ as associated with the interstitial oxygen O_I^{2-} (see section 3). Additionally, our calculations, which take into account various interactions, indicate that the spin–orbit (SO) interaction is the most important one compared with the two other magnetic interactions SS and SOO. The combined contribution to D from SS and SOO interactions is only 5.5%. The defect structure model obtained using the SPM-CFA/MSH approach reproduces very well the ranges of the experimental SH parameters D, $g_\parallel$ and $g_\perp$ as well as yields the correct magnitude and sign of D. Our investigations indicate that the experimental and theoretical SH parameters could be more precisely matched if more accurate experimental data, including EMR data on the fourth-rank ZFS parameters and/or crystal field energy levels not yet determined, become available.

Table 1. The CF and SH parameters (in units of cm^{-1}, except for the g factors) for the Fe_K^{3+}–O_I^{2-} defect center in $KTaO_3$ for various model assumptions and mechanisms considered; dash (—) means that the given parameter is not applicable here, whereas (N) means that no experimental data are available.

Parameter:	$(A)^a$	$(B)^b$	$(C)^c$	$(D)^d$	$(E)^e$	$(F)^f$	Experiment
B_{20}	—	−13 453.5	−13 453.5	16 750.3	18 445.0	19 941.3	N
B_{40}	−12 915.0	19 416.7	19 416.7	6051.1	19 481.9	18 112.1	N
B_{44}	−7718.2	28 175.7	28 175.7	4936.4	9345.3	8969.6	N
D	—	4.7278	4.4667	−0.1207	−0.3194	−0.3113	4.46 [9, 10]; 4.44 [5]; 4.3 [8]
$a + (2/3F)$	0.0006[g]	0.0541	0.0490	0.0001	0.0042	0.0036	N
$g_\parallel$	2.001 76	2.000 25	2.000 40	2.001 78	2.001 58	2.001 60	2.0 [9] ($g = 1.92$ [5])
$g_\perp$	2.001 76	1.997 06	1.997 37	2.001 80	2.001 63	2.001 65	2.0 [9]
$\Delta g(=g_\parallel - g_\perp)$	0	0.003 19	0.003 03	−0.000 02	−0.000 05	−0.000 05	N

[a] No displacement of Fe^{3+} ions, i.e. for $\Delta_1(Fe^{3+}) = 0$, no inward relaxation of the nearest oxygen O^{2-}, i.e. $\Delta_2(O^{2-}) = 0$, and absence of interstitial oxygens O_I^{2-}; with SO, SS and SOO.

[b] For $\Delta_1(Fe^{3+}) = 0.73$, $\Delta_2(O^{2-}) = 0.15$ (in units of $a/2$), and assuming the existence of interstitial oxygens O_I^{2-}; with SO, without SS and SOO.

[c] As (b); but with SO, SS and SOO.

[d] Calculated by us using the coordinates from the shell-model calculations of [37]; with SO, SS and SOO.

[e] Calculated by us using the coordinates from the generalized gradient approximation (GGA) for a 2 × 2 × 2 supercell (GGA-2)calculations of [76]; with SO, SS and SOO.

[f] Calculated by us using the coordinates from the generalized gradient approximation (GGA) for a 3 × 3 × 3 supercell (GGA-3) calculations of [76]; with SO, SS and SOO.

[g] The ZFS parameter F is not applicable.

Table 2. The coordinates of the Fe_K^{3+}–O_I^{2-} defect center in $KTaO_3$: (i) undistorted host, (ii) determined by us, (iii) the shell-model results and (iv) the generalized gradient approximation (GGA) for a 2 × 2 × 2 supercell (GGA-2) and a 3 × 3 × 3 supercell (GGA-3); in units of the lattice constant $a = 0.398\,85$ nm.

	Unrelaxed host			Our structural model		
Atom	x/a	y/a	z/a	x/a	y/a	z/a
Fe	0	0	0	0	0	0
O_I^{2-}	—	—	—	0	0	−0.4538
O_1	0.5000	0	0.5000	0.4250	0	0.1350
O_2	0.5000	0.5000	0	0.5000	0.5000	−0.3650
O_3	0.5000	0	−0.5000	0.5000	0	−0.8650

Shell model of [37]			Model GGA-2 of [76]			Model GGA-3 of [76]		
x/a	y/a	z/a	x/a	y/a	z/a	x/a	y/a	z/a
0	0	0	0	0	0	0	0	0
0	0	−0.4577	0	0	−0.4209	0	0	−0.4191
0.4496	0	0.2833	0.4797	0	0.2189	0.4820	0	0.2108
0.5015	0.5015	−0.1593	0.5095	0.5095	−0.2892	0.5114	0.5114	−0.2794
0.6136	0	−0.7159	0.5258	0	−0.7953	0.5260	0	−0.8051

Concerning other alternative models the following conclusions may be offered. Donnerberg *et al* [37] have determined the coordinates of the Fe^{3+}–O_I^{2-} defect center in $KTaO_3$ using the shell-model calculations. Leung [76] has determined the coordinates of the Fe^{3+}–O_I^{2-} defect center in $KTaO_3$ using the generalized gradient approximation (GGA) for a 2 × 2 × 2 supercell (GGA-2) and a 3 × 3 × 3 supercell (GGA-3). To check the predictions arising from alternative models, we have also calculated the SH parameters for the Fe^{3+}–O_I^{2-} defect center using the structural data provided in [37] and [76]. The values of D calculated in this way (table 1, cases (D), (E) and (F)) are very small and of the opposite sign as compared with the experimental EMR data [7], whereas the much smaller values of $(a + 2/3F)$ as compared with our model are obtained for the shell model and the two GGA models. To understand the differences between the approach [37, 76] and our method as well as the resulting SH parameters, in table 2 we provide the coordinates of the interstitial oxygen, Fe^{3+} ion, and the nearest oxygens for Fe^{3+}:$KTaO_3$. Using these coordinates we calculated the derived structural data for the Fe_K^{3+}–O_I^{2-} center in table 3. Due to the axial symmetry of the center, it is enough to specify the coordinates of only one representative oxygen for each plane. The coordinates (table 2) and the derived structural data (table 3) calculated by us differ substantially from those obtained in the shell model [37] and GGA [76] calculations. Additionally, in table 4 we provide the corresponding deviations, i.e. the off-center displacement of the Fe^{3+} ion Δ_1 and the inward relaxation of the nearest-neighbor (O_1–O_{12}) oxygens Δ_2, assuming that the upper oxygen (O_1–O_4) plane and the lower (O_9–O_{12}) plane are equally distant from the position of the K^+ ion in the

Table 3. The derived structural data for the Fe_K^{3+}–O_I^{2-} defect center in Fe-doped $KTaO_3$.

Type of data	Type of ligand	[37] Shell model	[76] GGA-2	[76] GGA-3	Present work
Bond length Fe-O_i (nm)	Upper oxygens O_1–O_4	0.211 94	0.210 31	0.209 83	0.177 86
	Middle oxygens O_5–O_8	0.289 90	0.309 67	0.309 24	0.317 39
	Lower oxygens O_9–O_{12}	0.376 06	0.380 26	0.383 57	0.398 50
	Interstitial oxygen O_I	0.182 57	0.167 88	0.167 16	0.181 00
Polar angle θ[a]	Upper oxygens O_1–O_4	57.8	65.5	66.4	72.4
	Middle oxygens O_5–O_8	102.7	111.9	111.1	117.3
	Lower oxygens O_9–O_{12}	139.4	146.5	146.8	150.0
Azimuthal angle φ[b]	Upper oxygens O_1–O_4	$\varphi_1 = 0°, \varphi_2 = 90°, \varphi_3 = 180°, \varphi_4 = 270°$			
	Middle oxygens O_5–O_8	$\varphi_5 = 45°, \varphi_6 = 135°, \varphi_7 = 225°, \varphi_8 = 315°$			
	Lower oxygens O_9–O_{12}	$\varphi_9 = 0°, \varphi_{10} = 90°, \varphi_{11} = 180°, \varphi_{12} = 270°$			

[a] The polar angle θ means the sharp angle between the Fe–O bond and the [001] axis.

[b] The data for the azimuthal angle φ are obtained only by us.

Table 4. The deviations (in units of $a/2$) predicted by various models: the off-center displacement of the Fe^{3+} ion Δ_1 and the inward relaxation of the nearest-neighbor oxygens in the upper oxygen (O_1–O_4) plane $\Delta_{21}(i)$, the middle (O_5–O_8) plane $\Delta_{22}(i)$ and the lower (O_9–O_{12}) plane $\Delta_{23}(i)$, calculated using data in table 1; for explanations see text.

	Δ_1	$\Delta_{21}(xy)$	$\Delta_{21}(z)$	$\Delta_{22}(xy)$	$\Delta_{22}(z)$	$\Delta_{23}(xy)$	$\Delta_{23}(z)$
Shell model	0.433	0.101	0.001	−0.004	−0.114	−0.227	−0.001
GGA-3	0.594	0.036	−0.016	−0.032	−0.036	−0.052	0.016
GGA-2	0.576	0.041	−0.014	−0.027	0.002	−0.052	0.014
Present model	0.730	0.150	0	0	0	0	0

undistorted host. For interpretation of the approaches [37, 76], we need to define also the inward relaxation of the nearest-neighbor oxygens in: (1) the upper oxygen (O_1–O_4) plane by the deviation $\Delta_{21}(i)$, (2) the middle (O_5–O_8) plane by $\Delta_{22}(i)$ and (3) the lower (O_9–O_{12}) plane by $\Delta_{23}(i)$, where $i = xy$ for the displacement towards the plane center and $i = z$ for the displacement along the z axis.

These intrinsic differences between the four structural models are responsible for the predicted incompatible values of the SH parameters. Further studies are needed to resolve the conditions of applicability and validity of various structural models as well as the underlying theoretical approaches. At present we can only offer tentative conclusions in this regard. Since the impurity ion Fe^{3+} carries extra charge as compared with the replaced host K^+ ion, the attractive force from Fe^{3+} acting on the nearest oxygen ligands, including the interstitial O_I^{2-}, is greater than that of the host ion K^+. Thus it may be expected that the nearest oxygens around the Fe^{3+} ion would move toward Fe^{3+} along the z axis. In fact, our results (table 2) show that the coordinate $|z/a|$ of the interstitial O_I^{2-} is smaller than 0.5000. This means that O_I^{2-} moves towards Fe^{3+} along the z axis. The result is consistent with the expectation based on the electrostatic interaction between Fe^{3+} and the nearest oxygen atom around Fe^{3+} as well as being also compatible with the large differences of the Fe^{3+} and K^+ ionic radii. Additionally, the calculations [37, 76] for the inward relaxation of the nearest oxygen atoms around Fe^{3+} yield non-zero $\Delta_{21}(z)$, $\Delta_{22}(z)$ and $\Delta_{23}(z)$ in table 4, which means that these oxygens move along the z axis. The inward relaxation of the nearest oxygen atoms (O_5–O_{12}) around Fe^{3+} yield also non-zero $\Delta_{22}(xy)$ and $\Delta_{23}(xy)$ in table 4, which means that these oxygens move in the xy plane. Hence, the structural data arising in the shell-model [37] and GGA [76] calculations differ from those considered in our model, thus yielding different SH parameters. Our calculations indicate that, for our choice of the input parameters used in SPM and MSH calculations (i.e. B, C, ξ_d, M_0, M_2, k and Dq and CF parameters), the positive $D > 0$ is obtained for $\Delta_1(\mathrm{Fe}) > 0.6$. Hence, with $\Delta_1(\mathrm{Fe}) < 0.6$ predicted by the approaches [37, 76], the negative $D < 0$ must be obtained (see table 1). Additionally, the value of $\Delta_{21}(O_{xy})$ is much smaller than our value, which also results in a reduction of the predicted value of D. The predictions of the models [37, 76] could possibly be reconciled with the experimental EMR data, as in the case of our results based on the defect structure model outlined above, provided the input SPM and MSH parameters would be chosen differently. Such modeling requires further extensive studies.

It is worth mentioning that recent theoretical *ab initio* and MSH studies suggest that some caution is pertinent concerning the capabilities and reliability of the structural modeling [37, 76]. Akbarzadeh *et al* [78] have found that

the large-scale atomistic simulations based on the local-density approximation (LDA) and GGA are not accurate enough to reproduce, even qualitatively, the observed anomalous properties of $KTaO_3$. Importantly, the study reveals that the low-temperature local structure of $KTaO_3$ is characterized by off-center atomic displacements. *Ab initio* calculations of the electronic and optical properties of $KTaO_3$ performed using density functional theory [79] yield only 'good overall agreement' between the calculated electronic structure and the VUV spectroscopy data. A density functional theory study [80] has revealed that the $Fe^{\frac{4}{2}}$ ($S = 3/2$) center in $KTaO_3$ may be more likely ascribed to a Fe^{+} impurity at a K^{+} site, although suffering an off-center motion along ⟨001⟩ directions, than to a Fe^{5+} ion at a Ta^{5+} site. Earlier studies of the defect structure for Mn^{2+} in $KTaO_3$ crystal from the calculation of EMR zero-field splitting have been critically commented on by Zheng [81]. Several mistakes in the theoretical MSH studies using SPM-calculated CF parameters as input for SH parameter formulae derived from perturbation theory have been pointed out. Zheng *et al* [82] have provided an alternative interpretation of the optical spectra for Fe^{3+} in $KTaO_3$ and proposed another assignment of transitions than that arrived at earlier by Bryknar *et al* [27].

5. Conclusions

We have theoretically investigated the local structure using the knowledge of the crystal field (CF) parameters and the spin Hamiltonian (SH) ones for the Fe_K^{3+}–O_I^{2-} center in $KTaO_3$ crystal. The SH parameters considered here include the zero-field-splitting (ZFS) parameters D and $(a + 2F/3)$ as well as the Zeeman g factors $g_\parallel$ and $g_\perp$. Our approach is based on the CF theory [17–21], superposition model (SPM) [21, 34–36] and the microscopic spin Hamiltonian (MSH) theory [22–26]. Calculations are facilitated using the extended CFA/MSH package [42, 43, 45] and the newly developed SPM module [83]. The combined SPM-CFA/MSH approach enables comprehensive modeling of the CF and SH parameters, which are affected by the variations in the structural parameters. Definitive conclusions concerning the adopted defect structure models may be obtained by matching the theoretical predictions with the experimental EMR and/or optical spectroscopy data for a given center in a particular host. Our method takes into account the spin–orbit interaction as well as the spin–spin and spin–other-orbit interactions omitted in previous studies. The SPM-CFA/MSH approach provides the ranges of the structural parameters that account best for the experimental SH parameters. No fitting in the sense of least-squares fitting is performed. Hence, the present modeling approach is in no way affected by the over-fitting problem, i.e. the mismatch between the greater number of the fitted parameters and the smaller number of experimental data used for fittings. Nevertheless, a note of caution is pertinent concerning the inherent limitations of the experimental EMR data available at present for the Fe^{3+}–O_I^{2-} defect center in $KTaO_3$. No experimental data on the fourth-rank ZFS parameters a and F is available as yet, whereas the accuracy of the g values is rather low. Hence, the set of reliable experimental SH parameters available for modeling is limited mainly to the ZFS parameter D. In spite of these external limitations, our theoretical SPM-CFA/MSH approach provides a useful and reliable tool for matching the available experimental structural, EMR and optical spectroscopy data with the corresponding theoretical predictions.

Using the SPM-CFA/MSH approach, the defect structure model that assumes reasonable ranges of values of the structural parameters, including (i) the off-center displacement of the Fe^{3+} ions $\Delta_1(Fe^{3+})$, (ii) the inward relaxation of the nearest oxygen ligands $\Delta_2(O^{2-})$ and (iii) the distance R_4 between the interstitial oxygen O_I^{2-} in the vicinity of the Fe_K^{3+} center and this Fe^{3+} ion in $KTaO_3$, enables reproducing very well the ranges of the experimental SH parameters D, $g_\parallel$ and $g_\perp$. The predicted values of $(a + 2F/3)$, for which no experimental data is available, fall also in the ranges determined for Fe^{3+} ions in similar compounds. Thus, the adopted defect structural model is corroborated by our theoretical results; even so the available experimental data [7–10] are not accurate enough to form an acid test of our theoretical predictions. Most importantly, application of our SPM-CFA/MSH approach to the proposed defect structure model yields not only the correct magnitude of D but also its sign. Considerations of the ways of experimental and theoretical determination of the sign of D enable us to solve the controversy [16] concerning the sign of D for the Fe_K^{3+}–O_I^{2-} center. It turns out that this controversy arises from the misinterpretation and/or neglect of the ample experimental EMR data [4, 6, 7, 13–15] by Zheng *et al* [16].

In short, the SPM-CFA/MSH approach proves capable of predicting the SH parameters for the adopted defect structure model of the Fe_K^{3+}–O_I^{2-} center in $KTaO_3$ crystal, which match well the experimental values. When more accurate experimental data becomes available, more reliable modeling of the structural parameters and thus the SH parameters may be carried out. The alternative structural models existing in the literature provide other modeling options. Comparison of the results concerning the microscopic SH parameters and the underlying structural parameters derived based on the present model and our theoretical approach with those calculated based on other alternative models show some discrepancies. Our approach is capable of modeling more SH parameters than other approaches proposed in the literature and, unlike those approaches, is based on the complete diagonalization method instead of the perturbation expressions. Hence, our comprehensive theoretical approach offers considerable advantages over other approaches. Comparison of our results with those arising from alternative models existing in the literature indicates also presumably higher reliability of our predictions. The physical appropriateness of any modeling depends primarily on the validity of the adopted structural model. While the structural model considered in this paper appears to be corroborated by our results, further detailed experimental structural and spectroscopic studies may help to resolve the advantages and disadvantages of various structural models.

Acknowledgments

This work has been partially supported by the Education Department Natural Science Foundation of Shaanxi Province

(05JK139), the Scientific Project Fund (2006K04-G29) and Baoji University of Arts and Science Key Research Grant (ZK2505) as well as the research grant from the Polish Ministry of Science and Tertiary Education in the years 2006–2009.

References

[1] Samara G A 2003 *J. Phys.: Condens. Matter* **15** R367
[2] Siegel E and Müller K A 1979 *Phys. Rev.* B **19** 109
[3] Hannon D M 1971 *Phys. Rev.* B **3** 2153
[4] Bursian V E, Vikhnin V S, Sochava L S, Kapphan S and Hesse H 1997 *Phys. Solid State* **39** 547
[5] Geifman K N, Golovina I S and Kozlova I V 1997 *Phys. Solid State* **39** 766
[6] Reyher H J, Hausfeld N and Pape M 2000 *J. Phys.: Condens. Matter* **12** 10599
[7] Laguta V V, Glinchuk M D, Bykov I P, Karmazin A A, Grachev V G and Tritskiĭ V V 1987 *Sov. Phys.—Solid State* **29** 1442
[8] Vugmeĭster B E, Glinchuk M D and Pechenyĭ A P 1984 *Fiz. Tverd. Tela* **26** 3389
Vugmeĭster B E, Glinchuk M D and Pechenyĭ A P 1984 *Sov. Phys.—Solid State* **26** 2036 (Engl. Transl.)
[9] Bykov I P, Glinchuk M D, Karmazin A A and Laguta V V 1983 *Fiz. Tverd. Tela* **25** 3586
Bykov I P, Glinchuk M D, Karmazin A A and Laguta V V 1983 *Sov. Phys.—Solid State* **25** 2063 (Engl. Transl.)
[10] Reyher H J, Faust B, Maiwald M and Pape M 1996 *Appl. Phys.* B **63** 331
[11] Faust B, Reyher H J and Schirmer O F 1996 *Solid State Commun.* **98** 445
[12] Sochava L S, Bursian V E and Razdobarin A G 2000 *Phys. Solid State* **42** 1640
[13] Laguta V V, Glinchuk M D, Karmazin A A, Bykov I P and Syrnikov P P 1985 *Fiz. Tverd. Tela* **27** 2211
Laguta V V, Glinchuk M D, Karmazin A A, Bykov I P and Syrnikov P P 1985 *Sov. Phys.—Solid State* **27** 1328 (Engl. Transl.)
[14] Glinchuk M D, Zaritskii I M, Pechenyi A P and Antimirova T V 1985 *Sov. Phys.—Solid State* **27** 2143
[15] Pechenyi A P, Glinchuk M D, Antimirova T V and Kleemann W 1992 *Phys. Status Solidi* b **174** 325
[16] Zheng W C, He L, Wu X X and Liu H G 2006 *J. Phys. Chem. Solids* **67** 1444
[17] Wybourne B G 1965 *Spectroscopic Properties of Rare Earth* (New York: Wiley)
[18] Mulak J and Gajek Z 2000 *The Effective Crystal Field Potential* (Amsterdam: Elsevier)
[19] Morrison C A 1992 *Crystal Fields for Transition-Metal Ions in Laser Host Materials* (Berlin: Springer)
[20] Wildner M, Andrut M and Rudowicz C 2004 Optical absorption spectroscopy in geosciences. Part I: Basic concepts of crystal field theory *Spectroscopic Methods in Mineralogy* (*EMU Notes Mineralogy* vol 6) ed A Beran and E Libowitzky (Budapest: Eötvös University Press) chapter 3, pp 93–143
[21] Andrut M, Wildner M and Rudowicz C 2004 Optical absorption spectroscopy in geosciences. Part II: quantitative aspects of crystal fields *Spectroscopic Methods in Mineralogy* (*EMU Notes in Mineralogy* vol 6) ed A Beran and E Libowitzky (Budapest: Eötvös University Press) chapter 4, pp 145–88
[22] Abragam A and Bleaney B 1986 *Electron Paramagnetic Resonance of Transition Ions* (Oxford: Clarendon) (1970 (New York: Dover))
[23] Mabbs F E and Collison D 1992 *Electron Paramagnetic Resonance of d Transition-Metal Compounds* (Amsterdam: Elsevier)
[24] Pilbrow J R 1990 *Transition-Ion Electron Paramagnetic Resonance* (Oxford: Clarendon)
[25] Rudowicz C 1987 *Magn. Reson. Rev.* **13** 1
Rudowicz C 1988 *Magn. Reson. Rev.* **13** 335 (erratum)
[26] Rudowicz C and Misra S K 2001 *Appl. Spectrosc. Rev.* **36** 11
[27] Bryknar Z, Potůček Z and Schulz H J 1999 *Radiat. Eff. Defects Solids* **149** 51
[28] Zheng W C and Wu S Y 2001 *Appl. Magn. Reson.* **20** 539
[29] Weast R C 1986 *CRC, Handbook of Chemistry and Physics* (Boca Raton, FL: CRC Press) p F164
[30] Zhou Y Y 1990 *Phys. Rev.* B **42** 917
[31] Sharma R R, Das T P and Orbach R 1966 *Phys. Rev.* **149** 257
[32] Sharma R R, Das T P and Orbach R 1967 *Phys. Rev.* **155** 338
[33] Sharma R R 1968 *Phys. Rev.* **176** 467
[34] Newman D J 1971 *Adv. Phys.* **20** 197
[35] Newman D J and Ng B 1989 *Rep. Prog. Phys.* **52** 699
[36] Newman D J and Ng B (ed) 2000 *Crystal Field Handbook* (Cambridge: Cambridge University Press)
[37] Donnerberg H, Exner M and Catlow C R A 1993 *Phys. Rev.* B **47** 14
[38] Zheng W C 1992 *Phys. Rev.* B **45** 3156
[39] Reyher H J, Faust B, Käding M, Hesse H, Ruža E and Wöhlecke M 1995 *Phys. Rev.* B **51** 6707
[40] Laguta V V, Glinchuk M D, Bykov I P, Rosa J, Jastrabik L, Savinor M and Trybula Z 2000 *Phys. Rev.* B **61** 3897
[41] Venturini E L and Samara G A 2005 *Phys. Rev.* B **71** 094111
[42] Rudowicz C, Yeung Y Y, Yang Z Y and Qin J 2002 *J. Phys.: Condens. Matter* **14** 5619
[43] Yang Z Y, Hao Y, Rudowicz C and Yeung Y Y 2004 *J. Phys.: Condens. Matter* **16** 3481
[44] Ma D P, Ma X D, Chen J R and Liu Y Y 1997 *Phys. Rev.* B **56** 1780
[45] Rudowicz C, Yang Z Y, Yeung Y Y and Qin J 2003 *J. Phys. Chem. Solids* **64** 1419
[46] Yang Z Y, Rudowicz C and Yeung Y 2004 *Physica* B **348** 151
[47] Yang Z Y, Rudowicz C and Yeung Y 2003 *J. Phys. Chem. Solids* **64** 887
[48] Blume M and Watson R E 1963 *Proc. R. Soc.* A **271** 565
[49] Blume M and Watson R E 1962 *Proc. R. Soc.* A **270** 127
[50] Febbraro S 1987 *J. Phys. C: Solid State Phys.* **20** 5367
[51] Febbraro S 1988 *J. Phys. C: Solid State Phys.* **21** 2577
[52] Yu W L and Rudowicz C 1992 *Phys. Rev.* B **45** 9736
[53] Kuang X Y 1987 *Phys. Rev.* B **36** 712
[54] Yeung Y Y and Rudowicz C 1992 *Comput. Chem.* **16** 207
[55] Yeung Y Y and Rudowicz C 1993 *J. Comput. Phys.* **109** 150
[56] Bramley R and Strach S J 1983 *Chem. Rev.* **83** 49
[57] Rudowicz C 1985 *J. Phys. C: Solid State Phys.* **18** 1415
Rudowicz C 1985 *J. Phys. C: Solid State Phys.* **18** 3837 (erratum)
[58] Hannon D M 1967 *Phys. Rev.* B **164** 336
[59] Rudowicz C and Budzyński P 2006 *Phys. Rev.* B **74** 054415
[60] Silver B L 1976 *Irreducible Tensor Methods* (New York: Academic)
[61] Laguta V V 1998 *Sov. Phys.—Solid State* **40** 1989
[62] Laguta V V, Zaritskii M I, Glinchuk M D, Bykov I P, Slipenyuk A M, Rosa J and Jastrabik L 1999 *Solid State Commun.* **110** 173
[63] Rudowicz C and Sung H W F 2001 *Physica* B **300** 1
[64] Rudowicz C 2008 *Physica* B **403** 1882
[65] Rudowicz C 2008 *Physica* B **403** 2312
[66] Zheng W C and Wu S Y 1999 *J. Phys.: Condens. Matter* **11** 3127
[67] Zhao M G, Xu J A, Bai G R and Xie H S 1983 *Phys. Rev.* B **27** 1516
[68] Fraga S, Karwowski J and Saxena K M S 1976 *Handbook of Atomic Data* (Amsterdam: Elsevier)

[69] Rudowicz C 1987 *J. Phys. C: Solid State Phys.* **20** 6033
[70] Newman D J, Pryce D C and Runciman W A 1978 *Am. Mineral.* **63** 1278
[71] Edgar A 1976 *J. Phys. C: Solid State Phys.* **9** 4304
[72] Yu W L 1994 *J. Phys.: Condens. Matter* **6** 5105
[73] Marusak L A, Messier R and White W B 1980 *J. Phys. Chem. Solids* **41** 981
[74] Wu S Y, Dong H N and Wei W H 2004 *Z. Naturf.* a **59** 203
[75] Sochava L S, Basun S A, Bursian V E, Razdobarin A G and Evans D R 2007 *Phys. Solid State* **49** 2262
[76] Leung K 2002 *Phys. Rev.* B **65** 012102
[77] Baranov P G *et al* 2006 *Phys. Rev.* B **74** 054111
[78] Akbarzadeh A R, Bellaiche L, Leung K, Íñiguez J and Vanderbilt D 2004 *Phys. Rev.* B **70** 054103
[79] Cabuk S, Akkus H and Mamedov A M 2007 *Physica* B **394** 81
[80] Trueba A *et al* 2008 *Phys. Rev.* B **78** 085122
[81] Zheng W C 2007 *Spectrochim. Acta* A **67** 694
[82] Zheng W C *et al* 2007 *J. Lumin.* **126** 91
[83] Gnutek P and Rudowicz C 2009 *J. Rare Earth* **27** 627